Scheme IV

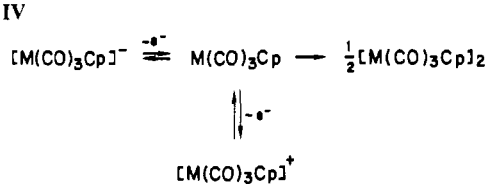

$(CO)_3\dot{C}p]^-$ and $[W(CO)_3Cp]^-$ in CH_3CN with 0.1 M TBAP. In both cases, oxidation of the anion (process II) leads to $[M(CO)_3Cp]^+$. The formation of the cation is demonstrated by the appearance of peak IV on the second negative potential sweep. This peak does not appear on the first negative sweep and thus suggests the reactions given in Scheme IV. The peak potential for the $[W(CO)_3Cp]^-/W(CO)_3Cp$ couple (reaction 14) is at −0.05 V in CH_3CN (Figure 3b) as compared to a peak potential of −0.72 V for the $[W(CO)_3Cp]^+/W(CO)_3Cp$ couple (reaction 13). Thus, at −0.05 V one would expect $[W(CO)_3Cp]^-$ to be oxidized directly to $[W(CO)_3Cp]^+$, and this is what is observed in Figure 3b. Likewise, thermodynamics also favor the formation of $[Mo(CO)_3Cp]^+$ from $[Mo(CO)_3Cp]^-$, and this is illustrated by the presence of peak IV in Figure 3a. In this regard, it should be noted that $[M(CO)_3Cp]_2$ is the product of both $[M(CO)_3Cp]^-$ oxidation and $[M(CO)_3Cp]^+$ reduction. Thus, the presence of both peaks IV and I in Figure 3 follows from the fact that the dimer is inevitably the only species at the electrode surface when potentials sufficiently negative to cause its reduction are reached.

A key point in Schemes I–IV is the presence of the $M(CO)_3Cp$ radical. This species is formed by oxidation or reduction of $[M(CO)_3Cp]_2$ as well as by oxidation of $[M(CO)_3Cp]^-$ or reduction of $[M(CO)_3Cp]^+$. A combined, overall oxidation–reduction mechanism for the interconversion of $[M(CO)_3Cp]_2$, $[M(CO)_3Cp]^-$, and $[M(CO)_3Cp]^+$ is presented in Figure 4. The importance of the $M(CO)_3Cp$ radical is clear. In addition to the major reaction pathways of $M(CO)_3Cp$, the reaction of O_2 with

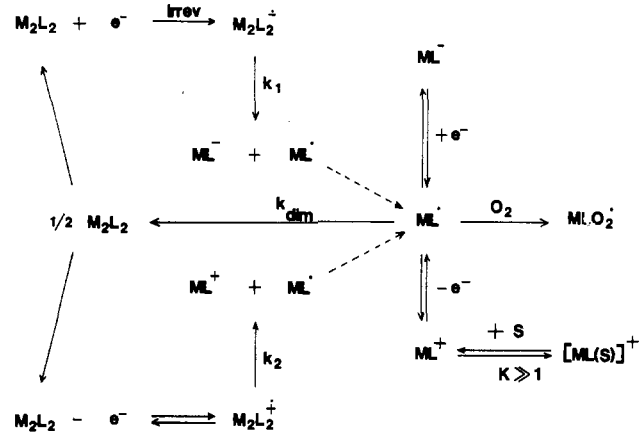

Figure 4. Overall mechanism for the electrochemical interconversion of $[M(CO)_3Cp]_2$, $[M(CO)_3Cp]^+$, $[M(CO)_3Cp]^-$, and $M(CO)_3Cp$ where M = Mo and W. These species are represented by M_2L_2, $[ML]^+$, $[ML]^-$, and ML.

the species is indicated. This reaction will particularly allow for indirect observation of $M(CO)_3Cp$ by ESR spectroscopy.[14] This scheme is similar to that reported for the oxidation and reduction of $Mn_2(CO)_{10}$,[18] and this similarity in the oxidation or reduction of three metal–metal-bonded dimers suggests that this type of mechanism may be general to systems of this type.

Acknowledgment. The support of the National Science Foundation (Grant CHE-8215507) is gratefully acknowledged. We also acknowledge helpful conversations with Dr. Paul Lemoine, who read a preliminary draft of the manuscript.

Registry No. $[Mo(CO)_3Cp]_2$, 12091-64-4; $[W(CO)_3Cp]_2$, 12091-65-5; $[Mo(CO)_3Cp]^-$, 12126-18-0; $[W(CO)_3Cp]^-$, 12126-18-0; $[Mo(CO)_3Cp]^+$, 12126-17-9; $[W(CO)_3Cp]^+$, 102262-08-8; $Mo(CO)_3Cp$, 12079-69-5; $W(CO)_3Cp$, 12079-77-5; Mo, 7439-98-7.

Contribution from the Department of Chemistry, The University of Houston—University Park, Houston, Texas 77004, and Laboratoire de Synthèse et d'Electrosynthèse Organométallique associé au CNRS (UA33), Faculté des Sciences "Gabriel", University of Dijon, 21100 Dijon, France

Electrochemical Studies of Dimeric Niobium(V) Porphyrins. Reactions of $[(OEP)Nb]_2O_3$ and $[(TpTP)Nb]_2O_3$ in Nonaqueous Media

J. E. Anderson,[1a] Y. H. Liu,[1a] R. Guilard,[1b] J.-M. Barbe,[1b] and K. M. Kadish*[1a]

Received November 18, 1985

The electrochemistry and spectroelectrochemistry of $[(P)Nb]_2O_3$, where P is the dianion of either octaethylporphyrin (OEP) or tetra-*p*-tolylporphyrin (TpTP), is reported in five different nonaqueous solvents. These Nb(V) dimers may undergo up to three reductions and three oxidations depending upon the solvent/supporting electrolyte system and temperature. ESR measurements on the bulk-electrolyzed solutions are combined with electrochemical and spectroelectrochemical data to present an overall electrooxidation/reduction mechanism for the two dimeric complexes.

Introduction

Monomeric Nb(V) porphyrins of the type (P)Nb(O)(X) and $(P)Nb(X)_3$ have been characterized, where P is the dianion of a given porphyrin macrocycle and X is a halogen.[2-6] The crystal structure of (P)Nb(O)(F)[7] and $(P)Nb(O)(O_2CCH_3)$[2] show that the Nb(V) atom is above the plane of the porphyrin ring and that the other axial ligands assume a cis geometry with respect to the porphyrin ring. The acetate group in $(OEP)Nb(O)(O_2CCH_3)$ is bidentate in the solid state. The same unusual geometry is also adopted by Nb(V) in $[(P)Nb]_2O_3$ where P = OEP, TPP, and TpTP.[2,8,9] These dimeric complexes have three oxygen atoms,

(1) (a) The University of Houston. (b) University of Dijon.
(2) Lecomte, C.; Protas, J.; Guilard, R.; Fliniaux, B.; Fournari, P. *J. Chem. Soc., Dalton Trans.* **1979**, 1306.
(3) Lecomte, C.; Protas, J.; Guilard, R.; Fliniaux, B.; Fournari, P. *J. Chem. Soc., Chem. Commun.* **1976**, 435.
(4) Buchler, J. W.; Rohbock, K. *Inorg. Nucl. Chem. Lett.* **1972**, *8*, 1073.
(5) Gouterman, M.; Hanson, L. K.; Khalil, G.-E.; Buchler, J. W.; Rohbock, K.; Dolphin, D. *J. Am. Chem. Soc.* **1975**, *97*, 3142.
(6) Green, M. L. H.; Moreau, J. J. E. *Inorg. Chim. Acta* **1978**, *31*, L461.
(7) Lecomte, C.; Protas, J.; Richard, P.; Barbe, J.-M.; Guilard, R. *J. Chem. Soc., Dalton Trans.* **1982**, 247.
(8) Johnson, J. F.; Scheidt, W. R. *J. Am. Chem. Soc.* **1977**, *99*, 294.

0020-1669/86/1325-2250$01.50/0

which bridge the two niobium porphyrin units. Only one oxygen is at an equal distance between the two Nb atoms, and the other two oxygens are spaced unequally. Thus, each niobium center is closely associated with one of the two unequally spaced oxygens.

Monomeric Nb(IV) porphyrins such as $(P)Nb(O)$,[10] $(P)Nb(X)_2$,[11] and their dioxygen adducts $(P)Nb(X)_2(O_2)$[12] and $(P)Nb(O)(O_2)$[13,14] have also been reported. The $(P)Nb(X)_2(O_2)$ complex has been described as a $Nb(V)-O_2^-$ species on the basis of ESR data,[12] and the structure for this complex is believed to be similar to that of the monomeric Nb(V) porphyrins, i.e. where the niobium atom is out of the plane of the porphyrin ring and the nonporphyrin ligands are in a cis geometry.

The same coordination geometry is found in monomeric and dimeric porphyrins. For this reason only mild conditions are needed to cleave the dimer and form the monomer. For example, treatment of dimeric $[(P)Nb]_2O_3$ with acetic acid will generate monomeric $(P)Nb(O)(O_2CCH_3)$ as shown in eq 1.[2,15] On the

$$[(P)Nb]_2O_3 + 2HO_2CCH_3 \rightarrow 2(P)Nb(O)(O_2CCH_3) + H_2O \quad (1)$$

other hand, dimeric $[(P)Nb]_2O_3$ may be formed by the reaction of monomeric (P)Nb(O) with oxygen, as shown in eq 2.[3,11,12]

$$2(P)Nb(O) + {}^1/_2O_2 \rightarrow [(P)Nb]_2O_3 \quad (2)$$

The electrochemical reduction of Nb(V) monomers has been reported to occur via three one-electron-transfer steps in THF[10,11] and CH_2Cl_2.[15] The electrochemical reduction of $[(TPP)Nb]_2O_3$ also occurs via three one-electron-transfer steps in CH_2Cl_2,[15] but the site of electron transfer is unclear. The addition of the first electron can occur at the Nb(V) metal, generating a mixed Nb(IV), Nb(V) dimer or, alternatively, the first electron may be added to the porphyrin π ring system giving a dimeric Nb(V) anion radical. A mixed Nb(V), Nb(IV) dimer is postulated to exist after photochemical reduction of $[(TpTP)Nb]_2O_3$,[13] but this species has not been identified after electrochemical reduction. Thus, one aim of this present study is to clarify these points.

In this paper, we report a detailed electrochemical, spectroelectrochemical, and ESR study of $[(OEP)Nb]_2O_3$ and $[(TpTP)Nb]_2O_3$ where OEP is the dianion of octaethylporphyrin and TpTP is the dianion of tetra-*p*-tolylporphyrin. No oxidations of dimeric niobium porphyrins have ever been reported in the literature nor has the reduction of $[(OEP)Nb]_2O_3$ or $[(TpTP)Nb]_2O_3$ ever been investigated. In this study, an electrooxidation/reduction mechanism is presented in which the importance of the homogeneous reactions of both the reduced and the oxidized species is demonstrated.

Experimental Section

Instrumentation and Methods. UV–visible spectra were recorded on an IBM 9430 spectrophotometer or a Tracor Northern 1710 holographic optical spectrometer/multichannel analyzer. Samples for ESR measurement were electrolyzed under an inert atmosphere by Schlenk techniques. The samples were transferred to ESR cells modified for use on a Schlenk line and immediately frozen in liquid nitrogen. ESR spectra were recorded on an IBM Model ED-100 electron spin resonance system. All spectrochemical measurements, with the exception of spectroelectrochemistry, were performed by Schlenk techniques. Cyclic voltammetric and polarographic measurements were obtained by using either an IBM EC225 voltammetric analyzer or an EG&G Princeton Applied Research Model 174A/175 polarographic analyzer/potentiostat. This latter instrument was coupled with an EG&G Model 9002A X-Y recorder for potential scan rates less than 500 mV/s or a Tektronix 5111 storage oscilloscope for scan rates equal to or larger than 500 mV/s.

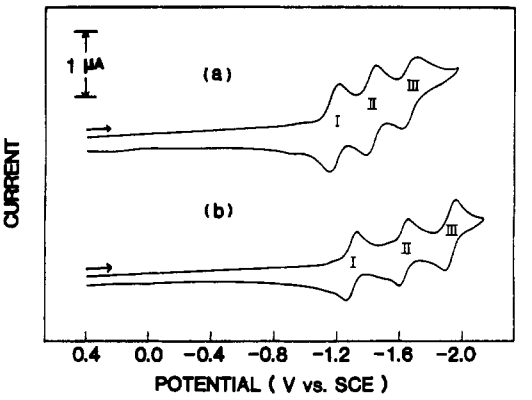

Figure 1. Cyclic voltammograms of (a) 5×10^{-4} M $[(TpTP)Nb]_2O_3$ at 22 °C in THF containing 0.2 M TBAP and (b) 5×10^{-4} $[(OEP)Nb]_2O_3$ at −78 °C in THF containing 0.2 M TBAP. Scan rate = 0.1 V/s.

The working and counter electrodes used were platinum. In the case of the thin-layer spectroelectrochemical cell, a platinum minigrid electrode was used. Potentials were all measured vs. a saturated calomel electrode (SCE), which was separated from the bulk of the solution by means of a fritted-glass-disk junction. Potential measurements were also made vs. the ferrocene/ferrocenium (Fc/Fc^+) couple for the purpose of evaluating liquid-junction-potential differences between solvents. Low-temperature experiments were performed by cooling the cell with a dry ice/acetone bath to a constant temperature, which was monitored with a thermocouple. Bulk controlled-potential coulometry was carried out on an EG&G Princeton Applied Research Model 173 potentiostat/model 179 coulometer system, coupled with a Shimadgu R-12 laboratory recorder or an EG&G Model RE 0074 time-based X-Y recorder. Thin-layer spectroelectrochemical measurements were made with an IBM EC225 voltammetric analyzer coupled with a Tracor Northern 1710 spectrometer/multichannel analyzer.

Materials. Solvents were purified for electrochemical and spectroscopic measurements by the following techniques: Reagent grade benzonitrile (PhCN) was vacuum distilled over P_2O_5 prior to use. Butyronitrile (*n*-PrCN) was predried with $CaCl_2$ and then distilled prior to use. Spectroscopic grade pyridine (py) was distilled from KOH. HPLC grade dichloromethane (CH_2Cl_2) was distilled from P_2O_5. Reagent grade tetrahydrofuran (THF) was distilled from Na and benzophenone. Tetra-*n*-butylammonium perchlorate (TBAP) was purchased from Eastman Kodak Co., twice recrystallized from ethyl alcohol, and stored in a vacuum oven at 40 °C. Unless otherwise noted, 0.2 M tetrabutylammonium perchlorate (TBAP) was used as a supporting electrolyte for cyclic voltammetric measurements, bulk solution electrolysis, and spectroelectrochemical measurements. The investigated metalloporphyrins, $[(OEP)Nb]_2O_3$ and $[(TpTP)Nb]_2O_3$, were synthesized and purified by methods already reported in the literature.[2]

Results and Discussion

Reduction of $[(P)Nb]_2O_3$. Figure 1 illustrates cyclic voltammograms of $[(TpTP)Nb]_2O_3$ and $[(OEP)Nb]_2O_3$ in THF with 0.2 M TBAP. The former compound gives well-defined voltammograms at room temperature (Figure 1a) while the latter complex undergoes one or more chemical reactions following electroreduction and the voltammograms are only reversible at −78 °C. The cyclic voltammogram of $[(OEP)Nb]_2O_3$ under these conditions is shown in Figure 1b.

As seen in Figure 1, both Nb(V) dimers are reduced by three reversible one-electron transfers on the electrochemical time scale. These are labeled processes I, II, and III in Figure 1, and for the case of $[(TpTP)Nb]_2O_3$, $E_{1/2} = -1.18$, -1.41, and -1.66 V at 22 °C. These three reductions are characterized by $|E_{pa} - E_{pc}|$ of 60 ± 5, 60 ± 5, and 90 ± 5 mV, respectively. $[(OEP)Nb]_2O_3$ is also reduced via three one-electron transfers, and at −78 °C, values of $E_{1/2} = -1.30$, -1.63, and 1.93 V are observed. These three reductions are characterized by $|E_{pa} - E_{pc}|$ at −78 °C of 60 ± 5, 60 ± 5, and 60 ± 5 mV, respectively. The fact that the values of $|E_{pa} - E_{pc}|$ are greater than what would be calculated for the reduced temperature and a Nernstian response reflects the effects of increased IR drop at lower temperatures. Two very small reduction waves are also observed at −78 °C. These occur at E_p

(9) Johnson, J. F.; Scheidt, W. R. *Inorg. Chem.* **1978**, *17*, 1280.
(10) Guilard, R.; Richard, P.; El Borai, M.; Laviron, E. *J. Chem. Soc., Chem. Commun.* **1980**, 516.
(11) Richard, P.; Guilard, R. *Nouv. J. Chim.* **1985**, *9*, 119.
(12) Richard, P.; Guilard, R. *J. Chem. Soc., Chem. Commun.* **1983**, 1454.
(13) Matsuda, Y.; Sakamoto, S.; Takaki, T.; Murakami, Y. *Chem. Lett.* **1985**, 107.
(14) Matsuda, Y.; Sakamoto, S.; Koshima, H.; Murakami, Y. *J. Am. Chem. Soc.* **1985**, *107*, 6415.
(15) Matsuda, Y.; Yamada, S.; Goto, T.; Murakami, Y. *Bull. Chem. Soc. Jpn.* **1981**, *54*, 452.

Table I. Potentials for Oxidation and Reduction of $[(OEP)Nb]_2O_3$ in Various Solvents Containing 0.2 M TBAP[a]

		redn			oxidn		
solvent	temp, °C	$E_{1/2}$, V	$E_{1/2}$, V	$E_{1/2}$, V	$E_{1/2}$, V	$E_{1/2}$, V	E_p,[b] V
THF	22	−1.29	−1.63	−1.92	0.78		
	−78	−1.30	−1.63	−1.93	0.72	1.12	
CH_2Cl_2	22	−1.40	−1.86		0.63	1.09	
	−40	−1.39	−1.86		0.63	1.20	
n-PrCN	22	−1.38	−1.80	−2.09	0.68	1.07	1.33
	−50	−1.37	−1.80	−2.13	0.68	1.04	1.37
PhCN	22	−1.43	−1.87		0.66	1.10	1.43
pyridine[c]	22	−1.41	−1.84		0.72		

[a] Only major peaks associated with $[(OEP)Nb]_2O_3$ are shown. Other peaks for reduced forms of (OEP)Nb(O) and other monomeric species are present depending on solvent and temperature. See text for details. [b] Scan rate = 0.1 V/s. [c] 0.1 M TBAP.

= −1.14 V and $E_{1/2}$ = −1.51 V and are due to the reduction of a small amount of monomeric Nb porphyrins that are formed by dissociation of the dimer.

Processes I–III have all the characteristics of diffusion-controlled reductions. The currents are proportional to the square root of scan rate, and values of E_p are invariant with increase in potential sweep rate. In addition, the anodic and cathodic peak heights for each process are approximately equal, suggesting identical one-electron transfers as shown in eq 3–5. A process involving

$$[(OEP)Nb]_2O_3 + e^- \rightleftarrows [[(OEP)Nb]_2O_3]^- \quad (3)$$

$$[[(OEP)Nb]_2O_3]^- + e^- \rightleftarrows [[(OEP)Nb]_2O_3]^{2-} \quad (4)$$

$$[[(OEP)Nb]_2O_3]^{2-} + e^- \rightleftarrows [[(OEP)Nb]_2O_3]^{3-} \quad (5)$$

two one-electron transfers to two identical, noninteracting sites on the dimeric compound is also characterized by $|E_{pa} - E_{pc}|$ = 60 mV. However, this possibility is ruled out in the present study due to the fact that currents for all oxidations and reductions are equal and the unlikelihood that 12 electrons could be added or abstracted in the six redox reactions while remaining noninteracting.

The cyclic voltammogram of $[(OEP)Nb]_2O_3$ in THF is different at room temperature than at −78 °C. This is demonstrated in Figure 2. Figure 2a illustrates a voltammogram of $[(OEP)Nb]_2O_3$ where the negative potential sweep is terminated at −1.46 V, while parts b and c of Figure 2 show the reduction of the same compound when the sweep is terminated at −1.80 and −2.10 V, respectively. For all three potential cutoffs, there is no change in the cathodic portion of the voltammogram. The three reduction peaks are still well defined in Figure 2b,c, but the oxidation currents for processes I–III are much reduced in intensity after the potential is swept to either −1.80 or −2.10 V. In addition, three new oxidation peaks appear at ~0.0, −1.1, and −1.47 V vs. SCE. These are labeled as peaks IV–VI in Figure 2c. Finally, Figure 2d shows the cyclic voltammogram of $(OEP)Nb(O)(O_2CCH_3)$ under the same solution conditions for which $[(OEP)Nb]_2O_3$ is reduced.

It is evident from Figure 2 and from results in the literature[11] that the anodic peaks at −1.10 V (peak V) and −1.47 V (peak VI) correspond to the oxidation of a monomeric porphyrin species. Very little formation of the monomer occurs when the potential is reversibly scanned from +0.40 to −1.46 V. This is shown in Figure 2a. However, if the potential is scanned past the second reduction peak (process II), the oxidation currents at E_p = −1.10 and −1.47 V indicate that substantial amounts of the monomer has been formed. Finally, when the potential is scanned past the third reduction (peak III), the oxidation peak at −1.10 V is larger still. This is shown in Figure 2c.

Similar results were observed for the reduction of $[(OEP)Nb]_2O_3$ and $[(TpTP)Nb]_2O_3$ in other nonaqueous solvents. This is shown in Figure 3. The TpTP complex gives reversible electron transfers in CH_2Cl_2, THF, and PhCN (Figure 3a), but the OEP complex rapidly decomposes after the addition of two or more electrons (Figure 3b). The electrochemical reactions are only slightly shifted in potential between the five solvents and the same major reduction processes (I–III) and coupled oxidation peaks (IV and V) are observed in THF and *n*-PrCN. Only two reductions are seen in CH_2Cl_2, py, and PhCN due to the limited potential window of these solvents. The reduction potentials in each solvent are listed in Table I for $[(OEP)Nb]_2O_3$ and Table II for $[(TpTP)Nb]_2O_3$. These tables also list the oxidation potentials of the two complexes in each solvent.

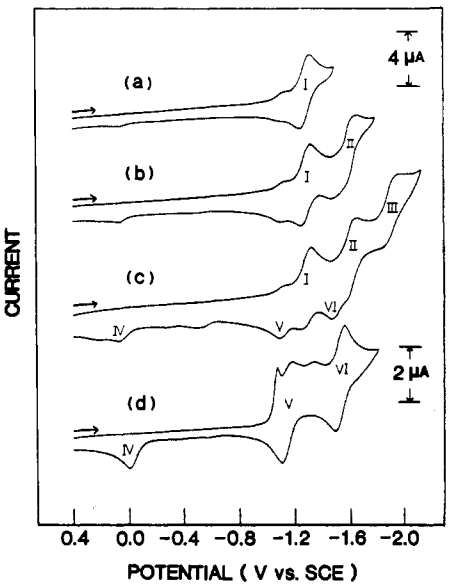

Figure 2. Room-temperature cyclic voltammograms of 8 × 10^{-4} M $[(OEP)Nb]_2O_3$ and 1.4 × 10^{-3} M $(OEP)Nb(O)(O_2CCH_3)$ in THF containing 0.1 M TBAP: (a) first reduction of dimeric $[(OEP)Nb]_2O_3$; (b) first two reductions of dimeric $[(OEP)Nb]_2O_3$; (c) first three reductions of dimeric $[(OEP)Nb]_2O_3$; (d) reductions of monomeric $(OEP)Nb(O)(O_2CCH_3)$.

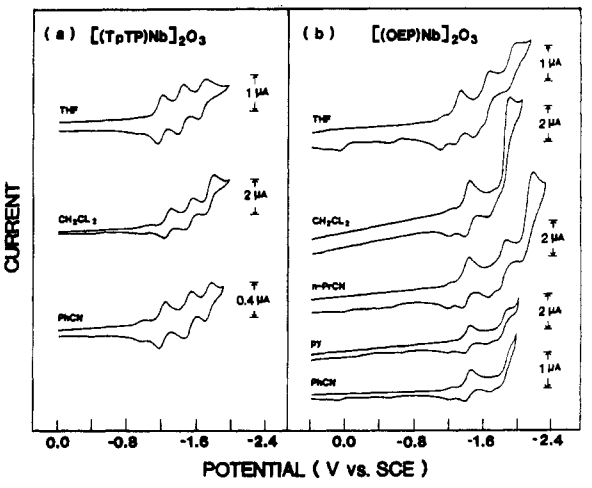

Figure 3. Cyclic voltammograms of (a) $[(TpTP)Nb]_2O_3$ and (b) $[(OEP)Nb]_2O_3$ in different solvents containing 0.2 M TBAP.

Site of Electroreduction. ESR measurements were performed on solutions of $[(OEP)Nb]_2O_3$ and $[(TpTP)Nb]_2O_3$ following bulk controlled-potential electrolysis in THF and are described below

Table II. Potentials for Oxidation and Reduction of $[(TpTP)Nb]_2O_3$ in Various Solvents Containing 0.2 M TBAP at 22 °C

	redn			oxidn	
solvent	$E_{1/2}$, V	$E_{1/2}$, V	$E_{1/2}$, V	$E_{1/2}$, V	E_p,[a] V
THF	−1.18	−1.41	−1.66	1.13[a]	
CH_2Cl_2	−1.28	−1.53	−1.75	0.89	1.20
PhCN	−1.21	−1.50	−1.73	0.94	1.22

[a] Irreversible reaction. Value presented is E_{pa} at a scan rate of 0.1 V/s.

for the reduction of $[(OEP)Nb]_2O_3$ at −1.34 and −1.50 V. These potentials are both negative of the first reduction at $E_{1/2}$ = −1.29 V (see Table I) but are positive of the second reduction at $E_{1/2}$ = −1.63 V. Thus, in both cases the addition of one electron is expected.

A free-radical signal is obtained when bulk electrolysis of $[(OEP)Nb]_2O_3$ is performed at −1.34 V. The signal has a g value of 2.001 and a width of 36 G and is assigned as being due to the first reduction product, $[[(OEP)Nb]_2O_3]^-$. The free-radical nature of the signal indicates that the electron is added primarily to a porphyrin ligand orbital and not to the Nb(V) atom as is postulated to occur during the photoreduction of $[(TpTP)Nb]_2O_3$.[13] The width of the ESR signal implies some interaction with the two niobium atoms, but no hyperfine splitting is observed.

In contrast to the above, three distinct successive ESR signals appear during controlled-potential reduction at −1.50 V. The form of these signals depends upon the total time of the bulk electrolysis. This is shown in Figure 4, which illustrates the ESR spectra obtained at various times during bulk electrolysis of $[(OEP)Nb]_2O_3$ in THF containing 0.2 M TBAP.

The signal in Figure 4a is the same free-radical signal that is observed after a controlled-potential reduction at −1.34 V. This signal remains up to the addition of approximately 1 faraday of electrons/dimer as determined by integration of the current–time curve. The second observed ESR signal (Figure 4b) is also a free-radical signal. It is centered at g = 2.004 and has a width of 10 G. This signal is always superimposed on the first or the third observed ESR signal, but the signal for this species increases in intensity as the original (first) signal decreases. The second signal is observed at the onset of a large current increase in the current–time curve during bulk electroreduction. This suggests that the ESR-active species is formed as a result of a chemical reaction that is initiated at −1.50 V. The third ESR signal obtained after a longer reduction at −1.50 V is shown in Figure 4c. This signal is observed before the second signal is totally lost, and the intensity of this signal continues to increase as that of the second signal decreases.

The ESR spectrum in Figure 4c is clearly due to a Nb(IV) species, and is similar to the signal reported for (OEP)Nb(O).[11] The second reduction potential for (OEP)Nb(O) has been reported to occur at $E_{1/2}$ = −1.60 V vs. SCE.[11] Thus, the ESR signal in Figure 4c can be ascribed to $[(OEP)Nb(O)]^{2-}$, which is generated in solution. This spectrum remains invariant if the applied potential is held constant at −1.50 V. However, upon bulk reoxidation of the solution at −1.00 V, a new ESR signal results, which is very similar to that shown in Figure 4c. This signal can be assigned as due to neutral (OEP)Nb(O), which is formed after the abstraction of two electrons from $[(P)Nb(O)]^{2-}$. Finally, after bulk reoxidation of the same solution at 0.00 V, all ESR signals disappear. At this potential, a Nb(V) species is formed as the product of the oxidation.

ESR measurements of reduced $[(TpTP)Nb]_2O_3$ give basically the same results as for reduced $[(OEP)Nb]_2O_3$. For example, when $[(TpTP)Nb]_2O_3$ is reduced at −1.22 V (0.2 M TBAP in THF), an initial free-radical signal is obtained. This signal has a g value of 2.002 and a width of 37 G. A second free-radical signal is also observed (g = 2.003 and a width of 22 G) at longer time scales of electrolysis, and a Nb(IV) species is invariably obtained after reduction at −1.50 V. The main difference between $[(TpTP)Nb]_2O_3$ and $[(OEP)Nb]_2O_3$ is that a more negative potential and longer time periods are necessary to observe the chemical conversion of reduced $[(TpTP)Nb]_2O_3$ to a form of (TpTP)Nb(O).

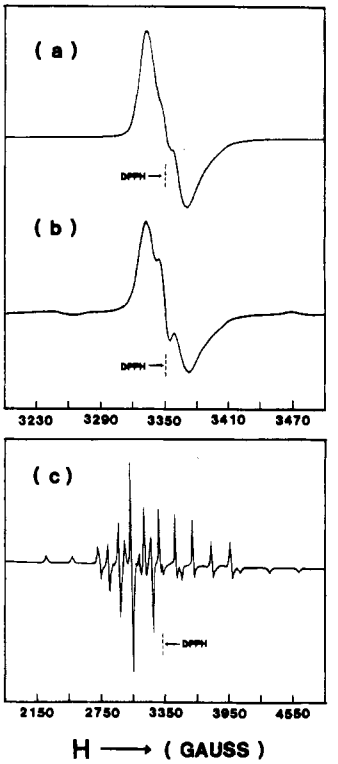

Figure 4. ESR spectra obtained during reduction of $[(OEP)Nb]_2O_3$ in THF containing 0.2 M TBAP: (a) signal after initial reduction at an applied potential of either −1.34 or −1.50 V; (b) signal after the addition of 1 faraday of electrons during controlled-potential reduction at −1.50 V; (c) final spectrum after controlled-potential reduction at −1.50 V.

Spectroelectrochemical measurements were taken during the stepwise reduction of $[(OEP)Nb]_2O_3$ and also demonstrate the existence of one or more chemical reactions following the first reduction. The original $[(OEP)Nb]_2O_3$ dimer is characterized by a Soret band at 399 nm and two bands in the visible region of the spectrum, which occur at 538 and 570 nm. When a controlled potential of −1.48 V is first applied to solutions of this compound, the Soret band decreases in intensity and shifts to 415 nm. The bands at 538 and 570 nm also decrease in intensity, and new bands appear at 631, 665, and 806 nm. These changes are shown in Figure 5a and suggest formation of a porphyrin π radical anion upon addition of the first electron to $[(OEP)Nb]_2O_3$. This assignment is consistent with the ESR results in Figure 4a. However, when a controlled potential of −1.48 V was applied for longer periods of time, the UV–visible spectrum changed. The Soret band at 415 nm and the band at 631 nm decreased in intensity. At the same time, the band at 806 nm increased in intensity and a new band appeared at 455 nm. This is shown in Figure 5b. Finally, when the potential was switched to −1.86 V (230 mV past peak II), the UV–visible spectrum changed as follows: The bands at 415 and 455 nm decreased in intensity and became broad. The bands at 631 and 806 nm also decreased in intensity, and new bands appeared at 581 nm and 769 nm. These changes are shown in Figure 5c, and the UV–visible spectral data is summarized in Table III.

When solutions of reduced $[(OEP)Nb]_2O_3$ are reoxidized at −1.0 V following prolonged reduction at either −1.48 or −1.86 V, the final UV–visible spectrum is characterized by bands at 408, 539, and 575 nm. This spectrum is different from that of the initial $[(OEP)Nb]_2O_3$ dimer, but is similar to that reported for (OEP)Nb(O).[10] Thus, the UV–visible data are self-consistent with the ESR data and imply that (OEP)Nb(O), or one of its reduced forms, is the primary species in solution after reduction and chemical reaction of $[(OEP)Nb]_2O_3$.

Oxidation of $[(P)Nb]_2O_3$. The oxidation of $[(P)Nb]_2O_3$ proceeds in up to three one-electron-transfer steps depending upon the

Table III. Absorption Maxima and Molar Absorptivities of Reduced $[(OEP)Nb]_2O_3$ in THF Containing 0.2 M TBAP

electrode reacn	λ_{max}, nm ($10^{-4}\epsilon$, M^{-1} cm^{-1})					
none	399 (21)	538 (1.6)	570 (3.4)			
redn for 5 min at −1.48 V	415 (15.7)	631 (1.9)	665 (0.7)	806 (1.2)		
redn for 10 min at −1.48 V	414 (13.4)	455 (6.0)	631 (1.3)	665 (0.5)	806 (1.7)	
redn for 5 or 10 min at −1.86 V	414 (8.2)	452 (4.8)	489 (1.7)	536 (1.5)	581 (2.9)	769 (3.5)

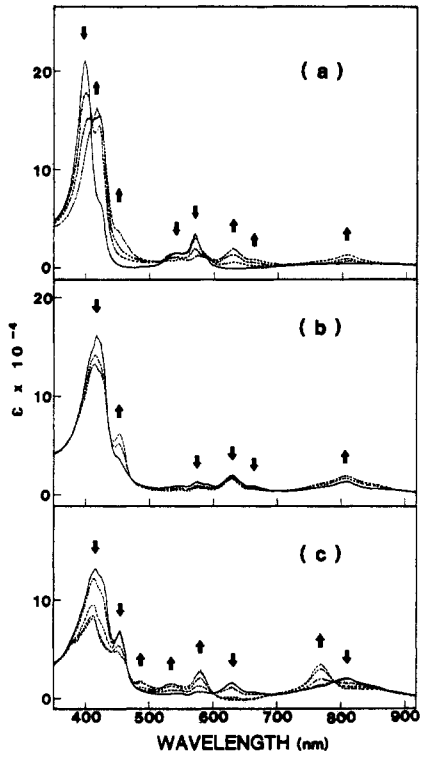

Figure 5. Thin-layer electronic absorption spectra of $[(OEP)Nb]_2O_3$ in THF containing 0.2 M TBAP: (a) during controlled-potential reduction at −1.48 V for 0–5 min; (b) after controlled-potential reduction at −1.48 V for 10 min; (c) after controlled-potential reduction at −1.86 V.

basicity of the porphyrin ring and the solvent system. This is shown in Figure 6, which illustrates room-temperature cyclic voltammograms of $[(OEP)Nb]_2O_3$ (Figure 6a) and $[(TpTP)Nb]_2O_3$ (Figure 6b) in five different nonaqueous solvents. Values of $E_{1/2}$ for oxidation of the two complexes in different solvents are presented in Tables I and II. As seen in these tables, the oxidation potentials for $[(TpTP)Nb]_2O_3$ are more positive than the oxidation potentials of $[(OEP)Nb]_2O_3$, reflecting the different basicities of the porphyrin rings.

Figure 7 shows the oxidation of $[(OEP)Nb]_2O_3$ in PhCN by rotating disk voltammetry (Figure 7a) and cyclic voltammetry (Figure 7b,c). The rotating disk voltammogram is characterized by three oxidation waves of equal current at $E_{1/2}$ = 0.66, 1.10, and 1.43 V. These oxidations are represented by eq 6–8. The

$$[(OEP)Nb]_2O_3 \rightleftharpoons [[(OEP)Nb]_2O_3]^+ + e^- \quad (6)$$

$$[[(OEP)Nb]_2O_3]^+ \rightleftharpoons [[(OEP)Nb]_2O_3]^{2+} + e^- \quad (7)$$

$$[[(OEP)Nb]_2O_3]^{2+} \rightleftharpoons [[(OEP)Nb]_2O_3]^{3+} + e^- \rightarrow \text{monomeric products} \quad (8)$$

first two oxidation process remain reversible if the positive potential scan is reversed before the third oxidation process (Figure 7b). These two oxidations are characterized by $|E_{pa} - E_{pc}| = 60 \pm 5$ mV and ratios of $i_p/v^{1/2}$ that are constant. This indicates that both peaks involve one-electron, diffusion-controlled processes. In contrast, the third oxidation of $[(OEP)Nb]_2O_3$ is followed by a chemical reaction that generates one or more monomeric Nb(V) species in solution. This is shown by the cyclic voltammogram in Figure 7c. As seen in this figure, three new waves are observed on the reverse scan (dashed lines) if potentials are scanned past

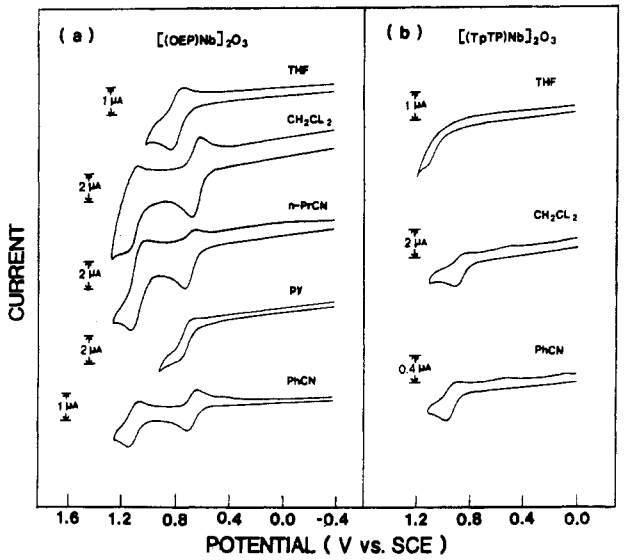

Figure 6. Cyclic voltammograms illustrating the oxidation of (a) $[(OEP)Nb]_2O_3$ and (b) $[(TpTP)Nb]_2O_3$ at room temperature in different solvents.

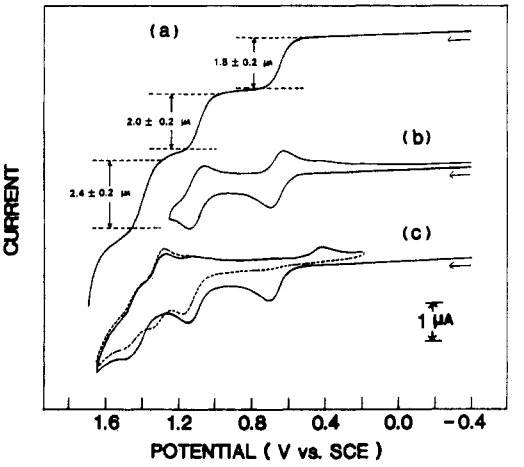

Figure 7. Oxidation of $[(OEP)Nb]_2O_3$ in PhCN, 0.2 M TBAP: (a) rotating disk voltammogram showing three oxidations; (b) cyclic voltammogram showing first two oxidations; (c) cyclic voltammogram showing all three oxidations.

the third oxidation wave. The first two processes are reversible and appear at $E_{1/2}$ = 1.13 V and $E_{1/2}$ = 1.30 V while the third new process is an irreversible re-reduction wave which occurs at 0.40 V. The same waves are also observed after $(OEP)Nb(O)(O_2CCH_3)$ has been doubly oxidized in PhCN[16] and indicate that the triply oxidized dimer must cleave to generate a monomeric species.

ESR measurements were carried out on frozen electrolyzed solutions of $[(OEP)Nb]_2O_3$ and indicate an oxidation at the porphyrin ring. If the solution is bulk electrolyzed at 0.8 V for 5 min, a free-radical signal is observed in the ESR, which is characterized by a g value of 2.004 and a width of 15 G. Thus, ESR measurements indicate that the first oxidation is ring-centered. If the controlled-oxidation potential is then increased to

(16) Anderson, J. E.; Liu, Y. H.; Guilard, R.; Barbe, J. M.; Kadish, K. M., submitted for publication.

1.3 V, the signal disappears, suggesting that a porphyrin dication is generated. However, after $[(OEP)Nb]_2O_3$ is electrolyzed at 1.3 V for 45 min, a new free-radical signal is observed at $g = 2.004$ with a width of 9 G. This is the signal of a monomeric Nb(V) porphyrin cation radical and demonstrates that decomposition of the dimer occurs even after the second oxidation by bulk electrolysis. This decomposition is not observed on the cyclic voltammetric time scale.

In conclusion, we have shown that the porphyrin niobium dimer $[(P)Nb]_2O_3$ can be reduced and oxidized in three one-electron-transfer steps. On the cyclic voltammetric time scale, the first reduction and the first two oxidations appear to be reversible. However, on longer time scales these electrode reductions are followed by chemical reactions whose ultimate product is a monomeric niobium porphyrin. Following reduction on long time scales, (P)Nb(O) or one of its reduced forms is the primary species in solution. The exact nature of the monomeric species following oxidation is not known at this time, but these products are presently being investigated. In later studies[16] we will present the detailed electrochemistry of several monomeric niobium(V) porphyrin species that are synthesized by literature techniques. The results from these studies will further develop the electrochemistry of the Nb porphyrin systems.

Acknowledgment. The support of the National Science Foundation (Grant CHE-8215507) is gratefully acknowledged. K.M.K. and R.G. also acknowledge the support of a joint NSF/CNRS collaborative research grant.

Contribution from the Stanford Synchrotron Radiation Laboratory and Departments of Applied Physics and Chemistry, Stanford University, Stanford, California 94305, and Department of Chemistry, University of Michigan, Ann Arbor, Michigan 48109

Polarized X-ray Absorption Near-Edge Structure of Highly Oxidized Chromium Porphyrins

James E. Penner-Hahn,[†‡] Maurizio Benfatto,[§∥] Britt Hedman,[†⊥] Tadashi Takahashi,[#] Sebastian Doniach,[§] John T. Groves,[#&] and Keith O. Hodgson*[⊥]

Received December 9, 1985

Polarized X-ray absorption near-edge spectra have been measured for Cr^{IV}(TTP)O and Cr^{V}(TTP)N (TTP is the dianion of 5,10,15,20-tetra-*p*-tolylporphyrin). These spectra, which are very similar for the two molecules, show an intense preedge absorption feature polarized perpendicular to the porphyrin plane. The absorption edges are relatively featureless when the polarization is parallel to the porphyrin plane. On the basis of multiple-scattered-wave Xα calculations, the intense preedge feature is interpreted as a bound → bound transition with significant metal character in the excited state. This transition, which has been observed in many metal-oxo species, was not observed in the putative ferryl (Fe=O) intermediates of horseradish peroxidase. The reasons for this absence in Fe=O species and its relationship to the reactivity of metal-oxo porphyrin complexes are discussed in light of the present results.

Introduction

When a core electron is excited with a sufficiently energetic photon, transitions to higher lying bound states and into the continuum are possible. For first-row transition metals, X-ray photons of energies from 4 to 9.6 keV have the appropriate energy to excite a 1s electron. The resulting X-ray absorption spectra are characterized by an abrupt increase in absorbance (the K absorption edge) at the excitation threshold. The absorption is frequently highly structured, both in the edge region and for 500–1000 eV above the edge. For the extended X-ray absorption fine structure (EXAFS) region (beginning about 50 eV above the edge), single scattering treatments give an adequate description of most of the structure.[1] In contrast, theoretical interpretation of edge spectra has proven difficult since in this region the long wavelength of the excited photoelectron permits extensive multiple-scattering interactions. Despite the theoretical difficulties, there is great interest in X-ray edge spectra since they can be quite sensitive to the detailed electronic structure and molecular geometry around the absorbing atom.

Recently, studies of polarization effects in single crystals have been used to simplify the interpretation of X-ray absorption edges.[2] Such measurements are possible as a result of the highly polarized nature (typically 95–99%) of synchrotron radiation.[3] For K absorption edges, the initial state is the totally symmetric 1s orbital; hence, the polarization properties of the edge structure are a direct reflection of the symmetry properties of the final state. This symmetry information provides additional information against which calculated edge spectra can be compared. In recent work, the combination of polarized measurements and multiple-scattered-wave Xα calculations has proven to be a useful tool for interpreting the X-ray absorption edge structure of Mo[4] and Cu[5] complexes. We report here the results of applying these experimental and theoretical approaches to the X-ray absorption edge spectra of two highly oxidized metalloporphyrin complexes.

Scheme I

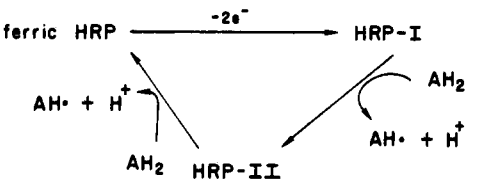

Metalloporphyrins are found at the active site of many metalloproteins. For the heme monooxygenase and peroxidase enzymes, a highly oxidized iron porphyrin is thought to be present at the active site. A particularly well-studied enzyme of this type is the peroxidase isolated from horseradish roots. The catalytic

* To whom correspondence should be addressed.
† Stanford Synchrotron Radiation Laboratory, SLAC, Bin 69, P.O. Box 4349, Stanford University.
‡ Present address: Department of Chemistry, University of Michigan, Ann Arbor, MI 48109.
§ Department of Applied Physics, Stanford University.
∥ Permanent address: Laboratori Nazionali Frascati INFN, Rome, Italy 00033.
⊥ Department of Chemistry, Stanford University.
Department of Chemistry, University of Michigan.
& Present address: Department of Chemistry, Princeton University, Princeton, NJ 08540.

(1) Lee, P. A.; Citrin, P. H.; Eisenberger, P.; Kincaid, B. M. *Rev. Mod. Phys.* **1981**, *53*, 796–806.
(2) Hahn, J. E.; Hodgson, K. O. *ACS Symp. Ser.* **1983**, *No. 211*, 431–444.
(3) Winick, H. *Synchrotron Radiation Research*, Winick, H., Doniach, S., Eds.; Plenum, New York, 1980; pp 11–25.
(4) Natoli, C. R.; Misemer, D. K.; Doniach, S.; Kutzler, F. W. *Phys. Rev. A* **1980**, *22*, 1104–1108.
(5) Smith, T. A.; Penner-Hahn, J. E.; Berding, M. A.; Doniach, S.; Hodgson, K. O. *J. Am. Chem. Soc.* **1985**, *107*, 5945–5955.

0020-1669/86/1325-2255$01.50/0